

Ultra-Efficient Resistance Switching between Charge Ordered Phases in 1T-TaS₂ with a Single Picosecond Electrical Pulse

Rok Venturini,^{1,2,*} Anže Mraz,^{1,3} Igor Vaskivskiy,¹ Yevhenii Vaskivskiy,^{1,2} Damjan Svetin,^{1,4} Tomaž Mertelj,¹ Leon Pavlovič,⁵ Jing Cheng,⁶ Genyu Chen,⁶ Priyanthi Amarasinghe,⁷ Syed B. Qadri,⁸ Sudhir B. Trivedi,⁷ Roman Sobolewski,^{6,9} and Dragan Mihailovic^{1,4,*}

¹*Jožef Stefan Institute, Jamova 39, Ljubljana, SI-1000, Slovenia,*

²*Faculty of Mathematics and Physics, University of Ljubljana, Jadranska 19, Ljubljana, SI-1000, Slovenia*

³*Faculty for Electrical Engineering, University of Ljubljana, Tržaška 25, SI-1000 Ljubljana, Slovenia*

⁴*CENN Nanocenter, Jamova 39, SI-1000 Ljubljana, SI-1000, Slovenia*

⁵*ELEP Electronics, Ljubljana, SI-1000, Slovenia*

⁶*Materials Science Program and Laboratory for Laser Energetics, University of Rochester, New York 14627, USA*

⁷*Brimrose Technology Corporation, Sparks, MD 21152, USA*

⁸*U.S. Naval Research Laboratory, Washington D.C., USA*

⁹*Department of Electrical and Computer Engineering and Department of Physics and Astronomy, University of Rochester, New York 14627, USA*

*Authors to whom correspondence should be addressed: rok.veturini@ijs.si and dragan.mihailovic@ijs.si

Progress in high-performance computing demands significant advances in memory technology. Among novel memory technologies that promise efficient device operation on a sub-ns timescale, resistance switching between charge ordered phases of 1T-TaS₂ has shown to be potentially useful for development of high-speed, energy efficient non-volatile memory devices. Measurement of the electrical operation of such devices in the picosecond regime is technically challenging and hitherto still largely unexplored. Here we use an optoelectronic “laboratory-on-a-chip” experiment for measurements of ultrafast memory switching, enabling accurate measurement of *electrical* switching parameters with 100 fs temporal resolution. Photoexcitation and electro-optic sampling on a CdMnTe substrate are used to generate and measure pulse propagation, with intra-band excitation and sub-gap probing, respectively. We demonstrate high contrast non-

volatile resistance switching of a 1T-TaS₂ device using *single* sub-2ps electrical pulses. Using detailed modeling we find that the switching energy density per unit area is exceptionally small, $E_A = 9.4 \text{ fJ}/\mu\text{m}^2$. The combined speed and energy efficiency place the 1T-TaS₂ devices into a category of their own amongst new generation non-volatile memory devices.

Memory speed and energy efficiency have become one of the major bottlenecks limiting advanced computer development.¹ As a result, there has been significant interest in recent years to address this issue by exploring novel memory concepts, such as memristors,² phase-change,³ ferroelectric⁴ and magnetic memory⁵ devices. One of the emerging new platforms for non-volatile storage of information is switching between distinct charge configurations of charge density wave (CDW) phases.^{6–11} Such phases are common in low-dimensional materials and have attracted a lot of interest from the point of view of fundamental physics as their formation is often not fully understood.^{12,13} When a CDW order in a material is disrupted, for example by the hydrostatic pressure^{14–16} or chemical doping,^{17–19} novel material functionalities can emerge, such as a large change of electrical resistance or an appearance of the superconducting state. Optical, THz, or electrical pulsed excitations can also be used to drive the material towards a novel charge order.^{6,7,20,21} However, the usefulness of such switching has long been limited, as excited CDW states are typically not stable, particularly at high temperatures.^{9,22,23}

The material used in this study is 1T-TaS₂, a layered transitional metal dichalcogenide. At room temperature, the material is in the metallic nearly commensurate (NC) CDW phase state, from which the insulating commensurate (C) CDW state forms below around 180 K.¹³ Either a laser or an electrical pulse excitation can drive the material from the insulating C state to the so-called metallic hidden (H) state with a complex pattern of domains separated by a network of domain walls.^{6,7,11,24,25} The H state is metastable and is not observed in the equilibrium phase diagram of the material. Owing to topological protection, the H state is remarkably stable at low temperatures.²⁵ Relaxation back to the C state is temperature dependent, but the state is stable on laboratory timescales at temperatures lower than 20 K.^{10,26,27} Robust memory device operation by switching between the two phases by electrical pulses of various lengths has already been demonstrated.^{7,10,11} Optical experiments show that once the transition between the charge ordered phases is triggered, it can stabilize into the new order within 400 fs.²⁷ If picosecond *electrical* pulses could trigger the resistance-switching charge reconfiguration it may be possible to write to such memory devices at THz frequencies. Due to limitations of

electrical generators and dispersion of cryostat cables, demonstration of electronic device operation on a such short timescale is currently still challenging.

A way to overcome these issues is by *in-situ* generation and detection of ultrashort electrical pulses on-a-chip by femtosecond laser pulses and then propagating electrical pulses along a coplanar transmission line (TL) to the device. While this technology is well known^{28–31} and has been used to perform switching of superconducting Josephson junctions³² and circuits,^{33,34} interest in this topic has recently re-emerged with ultrafast electronic studies of topological states of matter^{35,36} and magnetization reversal.^{37,38} In our case, we embedded a $1T$ -TaS₂ device in the TL on a substrate that is both photoconductive and exhibits an electro-optic (EO) effect so, in addition to the DC resistance measurement, ultrashort electrical pulses can be generated and sampled anywhere along the TL. The EO detection can easily be calibrated to a known voltage, so the measured picosecond pulse voltage can be used to calculate the pulse energy. This offers a significant advantage over experiments that use either a photoconductive gap or an antenna for detection, where calibration is difficult and the energy for switching can only be given as the upper limit estimate.^{37,38}

Figure 1 (b) shows a schematic of the lab-on-a-chip TL circuit used in our experiment. First, a 32 nm thick flake, exfoliated from bulk $1T$ -TaS₂ crystal, is deposited on the substrate. Next, the TL circuit is lithographically fabricated on top by deposition of 3 nm of Cr followed by 160 nm of Au. The three electrodes are marked A, B and C, where A is grounded, B is used to source DC voltage and C is used to measure the resistance of the $1T$ -TaS₂. TL electrodes A and B are 12 μ m wide and 34 μ m apart. The $1T$ -TaS₂ flake is positioned 100 μ m from the C electrode, with the TL gap of 0.6 μ m above the flake. The crucial part of the circuit is the 22 μ m wide gap between the electrodes B and C that acts as a capacitor, which prevents the DC current flow through the $1T$ -TaS₂ flake when a DC bias voltage is applied between leads A and B. At the same time, it allows the short photogenerated electrical pulses to be transmitted with low attenuation. The entire TL is 4 mm long (not shown) to reduce the effect of pulse reflections from the ends.

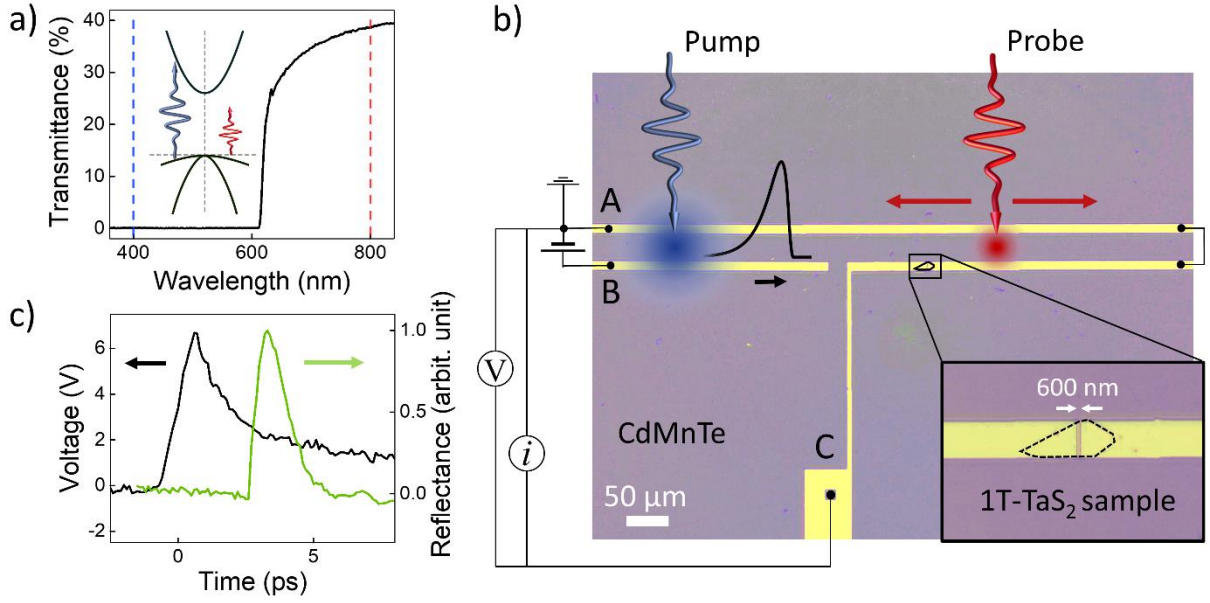


FIG. 1. (a) The absorption spectrum of the CMT in relation to the pump beam (blue) and the probe beam (red). An inset shows a schematic of the CMT band structure around $k=0$.³⁹ (b) A microscope image of the fabricated TL circuit over the exfoliated 1T-TaS₂ flake with the pump beam (blue) and the span of the probe beam (red) positions. The voltmeter and the current source are used for measurement of the flake resistance. The voltage source provides a DC bias voltage for electrical pulse generation. The inset shows a zoomed-in view of the 1T-TaS₂ flake in the circuit. (c) The transient reflectivity measurement of the CMT substrate by spatially overlapping both beams away from the TL circuit (green) is shown together with the picosecond electrical pulse that is detected by positioning the probe beam 40 μm in front of the 1T-TaS₂ flake and the pump beam between the electrodes A and B (black).

To facilitate both electrical pulse generation and electro-optical detection on the same substrate, we use a vanadium-doped $\text{Cd}_{0.55}\text{Mn}_{0.45}\text{Te}$ (CMT) single crystal substrate grown by the vertical Bridgman method.⁴⁰ CMT is a semiconductor with a 2.02 eV wide band gap that allows photocarrier generation using optical photons with $\lambda < 600$ nm, while transmitting red and longer wavelength photons ($\lambda \geq 700$ nm). The optical transmittance of the CMT substrate is shown in Fig. 1(a).

Vanadium doping results in highly resistive crystals with a short carrier lifetime. The area between electrodes A and B that is used as a photoswitch shows ohmic behavior without laser illumination with a resistance greater than 10^9 ohm. The photoexcited carrier lifetime,

determined using two-color (400 nm/800 nm) femtosecond pump-probe transient reflectivity (shown in Fig. 1(c)), is below 2 ps.

In addition, the CMT substrate has an EO tensor component along the [001] direction so the photogenerated electric-field transient propagating along the TL fabricated on the (110) plane can be measured via the Pockels effect.³¹ We can thus sample the propagating electric fields by an 800 nm, intra-gap (1.55 eV) laser beam focused between the TL coplanar lines in the transmission mode (see Fig. 1 (a)). Both the excitation of the picosecond electrical pulses by the 400-nm (3.1 eV) pump and the EO sampling by the 800-nm probe is done with ~ 100 fs long laser pulses at a 250 kHz repetition rate. An acousto-optic modulator positioned in the laser beam allows for single pulse picking, when necessary. The temporal evolution of the electrical pulses is measured by adjusting the time delay between the pump and probe pulses.

We first present room-temperature characterization of the picosecond electrical pulses generated in the TL circuit Fig. 1(b). A slightly defocused pump laser beam is used to illuminate the CMT substrate between electrodes A and B. Using a low laser fluence of 0.3 mJ/cm^2 and a moderate DC voltage of 76 V between the electrodes, we focus the probe beam $40 \text{ }\mu\text{m}$ from the $1T\text{-TaS}_2$ flake to give an accurate measurement of the electrical pulse shape propagating across the device. In this configuration, the full width at half maximum (FWHM) of the electrical pulse is measured to be 1.9 ps as shown in Fig. 1(c). Repeating the experiment with the probe beam on the other side, $100 \text{ }\mu\text{m}$ from the $1T\text{-TaS}_2$ crystal, we observe that the pulse shape is unaltered Fig. 3(a) but the amplitude is slightly smaller due to high-frequency losses.³¹

For ultrafast resistance switching of the $1T\text{-TaS}_2$ device, the chip is cooled from room temperature to 16 K, while the DC resistance of the device is continuously measured (Fig. 2). At 16 K we position the pump beam between the TL electrodes A and B, as before, and the probe after the $1T\text{-TaS}_2$ crystal. We measure the propagating electrical pulse shape with low DC bias voltage to verify that the pulse shape is unchanged. We then increase the DC voltage bias to 220 V without pump illumination. Using a single optical pump pulse with the fluence of 5.5 mJ/cm^2 from an acousto-optic pulse-picker, we now excite a single electrical switching pulse. After exposure we observe a large drop of the device resistance as shown in Fig. 2 (black arrow). This is consistent with resistance switching observed previously using longer electrical pulses.^{7,8} During heating of the crystal back to room temperature we observe an increase of the sample resistance between 50 K and 100 K corresponding to the relaxation of the metastable

H state back to the C state.^{6,26} The cycle of cooling - switching - erasing was sequentially repeated many times, demonstrating consistency of single-shot ultrafast resistance switching.

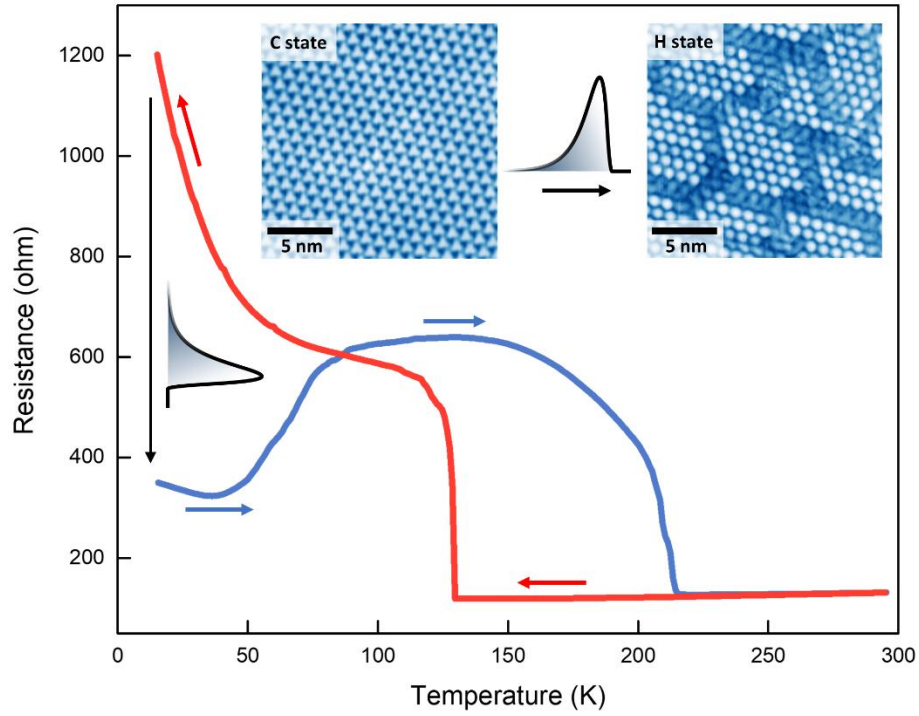


FIG. 2. Resistance of the 1T-TaS₂ flake upon cooling (red), resistance switching of the flake by a single 1.9 ps electrical pulse at 16 K (black arrow) and heating of the flake back to room temperature (blue). The insets are scanning tunneling microscope images of the C state (left) and the H state (right).

In all further switching experiments the temperature is kept below 20 K with the 1T-TaS₂ device operation in non-volatile mode. Next, we investigate how the single pulse switching resistance drop depends on the picosecond electrical pulse amplitude. We vary the pulse amplitude by either changing the DC bias voltage or the pump fluence. As expected, the pulse amplitude (at a fixed pump fluence of 0.4 mJ/cm²) increases almost linearly with increasing the DC voltage as shown in Fig. 3(c) (blue), while by varying the pump fluence (at a fixed DC bias voltage of 60 V) a sublinear dependence is observed, as shown in Fig. 3(d) (blue), consistent with previous results for the CMT substrate.³¹ Furthermore, no change in the shape of the picosecond pulse is observed by changing the DC bias and/or the pump fluence within the explored intervals of 0-250 V and 0-5.5 mJ/cm², respectively. In both cases we observe that the flake resistance remains unchanged for the picosecond pulse amplitudes below a DC bias threshold of ~70 V while above the threshold, it continuously decreases with increasing electrical-pulse amplitude, as shown in Fig. 3 (c) and (d).

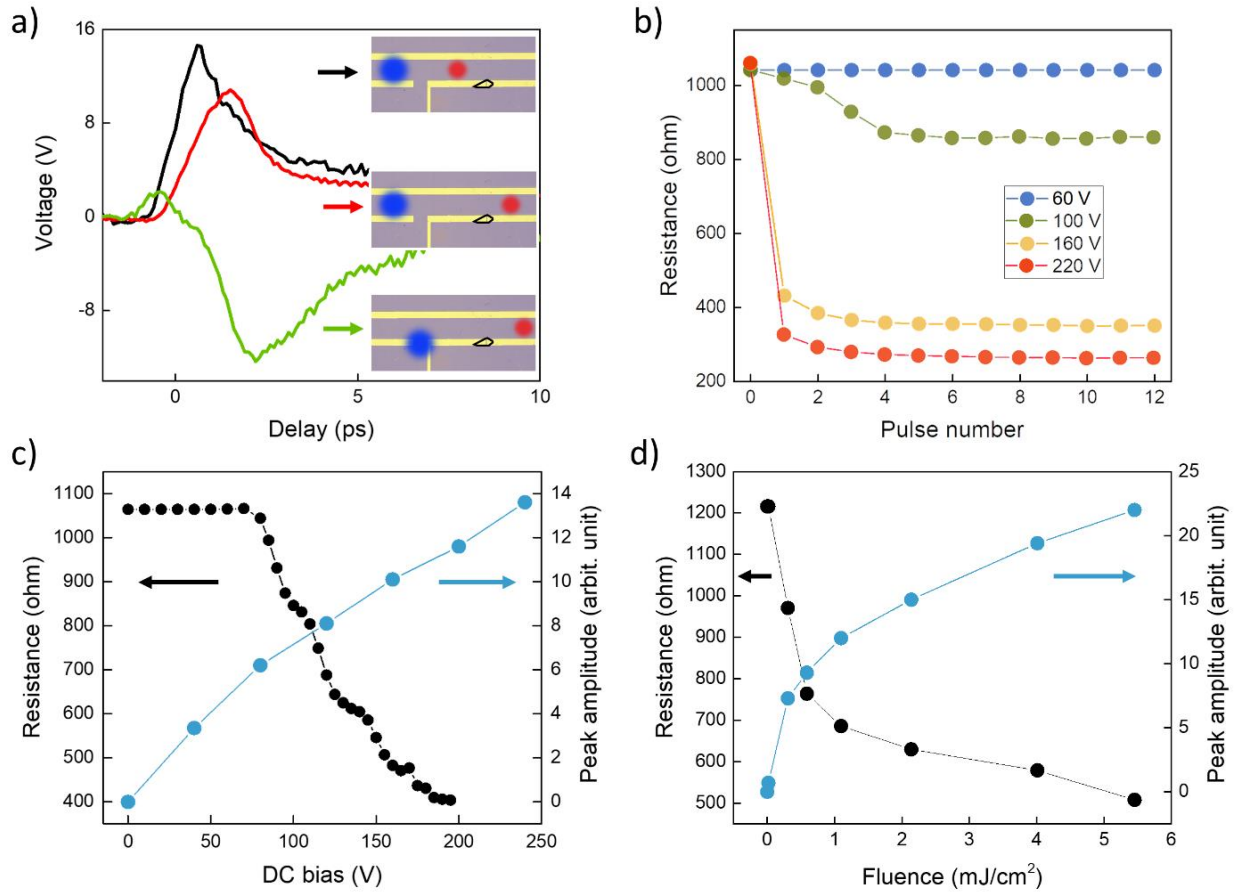


FIG 3. (a) The shape of the picosecond electrical pulse sampled by the probe beam 40 μm before (black) and 100 μm after the sample (red). An electrical pulse with a reversed polarity with the pump beam on a gap (green). Inset figures show the optical microscope image of the TL with the schematic of the pump (blue) and probe (red) beam positions. (b) Build-up effect on the 1T-TaS₂ resistance by applying multiple electrical pulses one by one at different DC bias voltages. (c) The electrical resistance of the 1T-TaS₂ flake (black) and picosecond pulse amplitude (blue) in relation to the DC bias at the constant pump fluence. (d) The electrical resistance of the flake (black) and excited picosecond pulse amplitude (blue) in relation to the pump fluence at the constant DC bias.

Further, we investigate the 1T-TaS₂ flake resistance changes in response to repeated single-pulse excitation at different DC bias voltages. After each single-pulse exposure we measure the resistance and wait 1 min before applying the next pulse. As shown in Fig. 3(b), the largest resistance drop is observed after the initial pulse, with the next few pulses gradually lowering the resistance towards saturation. Below the threshold, we do not observe any change in the flake resistance irrespective of the number of the applied pulses. Even after applying 10^8 pulses at a 250 kHz repetition rate below the threshold, at 60 V DC bias, there was no detectable

resistance change of the device. This demonstrates that the threshold for switching onset is very sharp and the device behavior is robust even for such short pulses.

Finally, we perform a slightly modified electrical switching experiment where instead of focusing the pump beam between electrodes A and B we focus it in the gap between electrodes B and C as shown in Fig. 3(a). We observe a similar pulse shape with the reversed polarity. Repeating the switching experiment with the electrical pulses of the reversed polarity we obtain a very similar switching behavior.

From Fig. 3(a) it is clear that only a small fraction of the picosecond pulse energy is absorbed in the 1T-TaS₂ flake while the majority of the pulse propagates along the TL past the flake. A large random spot-to-spot variation of the EO signal (~30%) prevents us from accurately measuring the very small dissipated energy in the 1T-TaS₂ flake by directly comparing the incident and transmitted EO signal energies. Instead, to estimate the energy of switching of the 1T-TaS₂ flake, we employ a 3D electromagnetic simulations software (Ansys HFSS) which allows us to numerically determine scattering parameters and impedance of the circuit. First, we simulate a straight coplanar TL without any gaps and the flake. For the CMT substrate we take the dielectric constant obtained in the parent compound.⁴² From the simulation we obtain the TL impedance of 125 ohms and the pulse propagation velocity of $c = 1.25 \times 10^8$ m/s. The calculated velocity is close to the measured one of 1.2×10^8 m/s. Using the calculated impedance and the experimentally measured pulse voltage between the electrodes we calculate the energy of the propagating picosecond electrical pulse at the threshold for switching, $E_T = \int \frac{U_{TL}^2(t)}{Z} dt = 0.59$ pJ, where U_{TL} is the voltage between the TL electrodes and Z is the impedance of the TL. The integral is extended to 7 ps after the pulse start to include also the pulse tail.

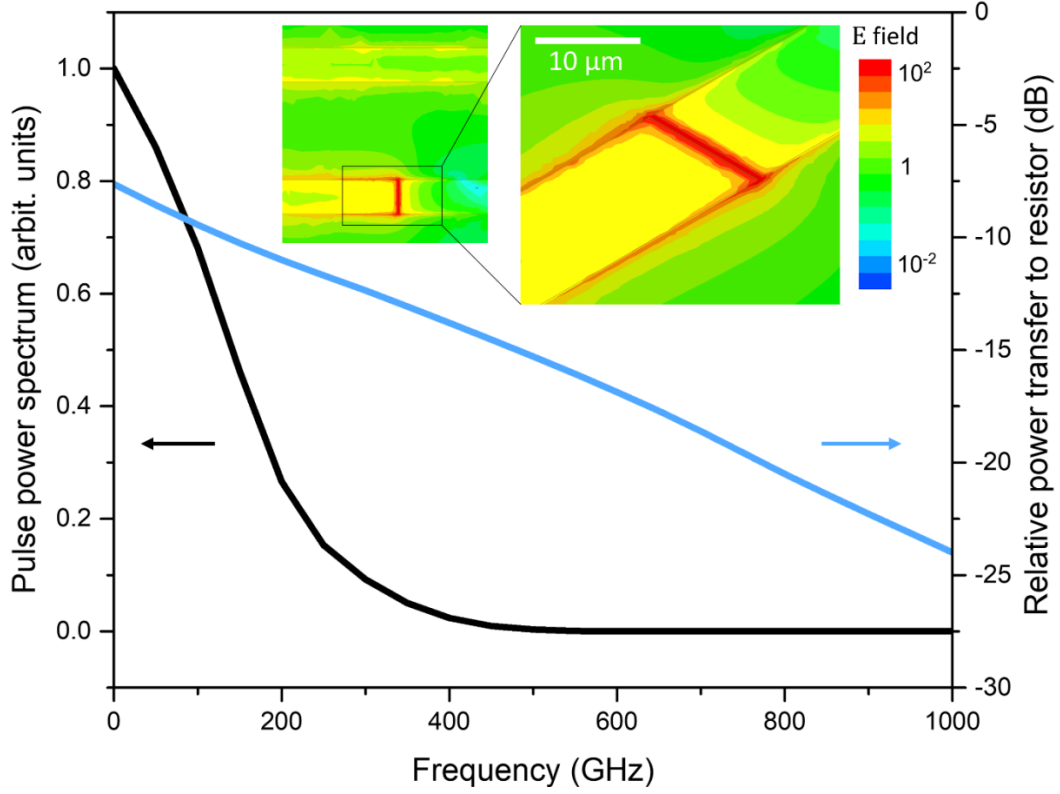


FIG. 4. The power spectrum of the picosecond electrical pulse (black) and the relative power transfer of the propagating pulse to the $1T$ -TaS₂ flake obtained from the simulation (blue). The insets show the calculated electric field relative to the field between TL electrodes simulated at the 100 GHz frequency.

Next, to estimate the relative absorbed energy, we modify the TL in the simulation by inserting a 600 nm gap using a 1100 ohm 2D resistor to represent the $1T$ -TaS₂ flake in the high resistance state (see inset to Fig. 4). The simulated relative power transfer to the resistor inside the gap is found to be small and strongly frequency dependent (see Fig. 4). The experimental dissipated energy is then estimated by multiplying the experimental picosecond electrical pulse power spectrum (Fig. 4) by the simulated power-dissipation spectrum in the resistor and integrating over the frequency. We find that only 11.5 % of the electrical pulse energy is dissipated in the $1T$ -TaS₂ flake. For the electrical pulse amplitude at the switching threshold, this corresponds to switching energy of 68 fJ. Note that this is an upper bound since it assumes that all the energy is dissipated in the switching process. Optical experiments indicate that the transition to a low resistance state is triggered already within 400 fs after the optical pulse arrival, which indicates that only the first part of the electrical pulse might be responsible for switching and the energy from the tail of the electrical pulse only contributes to heating of the already switched device.

By using the dimensions of the 1T-TaS₂ flake between the electrodes, the estimated switching energy of 68 fJ corresponds to an energy density per unit volume $E_V = 0.3 \text{ pJ}/\mu\text{m}^3$, or an energy per unit area $E_A = 9.4 \text{ fJ}/\mu\text{m}^2$. Thus, to our best knowledge, 1T-TaS₂ devices exhibit the lowest switching energy per unit area and the fastest switching time for any fast memory device reported.¹⁰ Considering the large size of the device used in the present experiments, the energy for resistance switching could potentially be reduced by more than an order of magnitude by fabricating smaller devices.

To conclude, our lab-on-a-chip experiments demonstrate that the non-volatile switching with a large resistance contrast is possible in 1T-TaS₂ devices approaching terahertz speeds, presently limited only by the substrate carrier lifetime. Direct, high temporal resolution measurements of the pulse propagation on the transmission line circuit are the key for demonstrating ultrafast and energy efficient switching, approaching the optical 400 fs switching limit.²⁷

Considering that the devices operate well at low temperatures, the charge configuration memory elements based on the resistance switching in 1T-TaS₂ could fit well with the emerging technologies that operate at cryogenic temperatures and lack a suitable memory device.⁴³ Due to ultra-high switching speed, one obvious match is the superconducting single-flux-quantum (SFQ) logic, which relies on picosecond long SFQ pulses to process data.⁴⁴ With the ability to grow few-layer crystals by epitaxial growth,^{45,46} devices based on the charge configuration switching could provide a much-needed ultrafast and energy efficient solution for the classical information storage in both the classical and quantum computing environments.

Conflict of interest: The authors declare no competing interests.

Acknowledgment

The authors would like to thank Jan Ravnik for his help with building the optical setup. The work at the Jožef Stefan Institute was supported by the Slovenian Research Agency (No. P1-0040, No. N1-0092, No. J1-2455, R.V. to No. PR-10496, A.M. to No. PR-08972, D.S. to No. I0-0005), Slovene Ministry of Science (No. Raziskovalci-2.1-IJS-952005), and ERC PoC (No.GA767176). The work in Rochester and Brimrose was supported by the DOE STTR 2021 Phase 1 grant # DE-SC0021468. We thank the CENN Nanocenter for the use of the AFM and the FIB.

- ¹ M.A. Zidan, J.P. Strachan, and W.D. Lu, *Nat Electron* **1**, 22 (2018).
- ² S. Pi, C. Li, H. Jiang, W. Xia, H. Xin, J.J. Yang, and Q. Xia, *Nat. Nanotechnol.* **14**, 35 (2019).
- ³ D. Loke, T.H. Lee, W.J. Wang, L.P. Shi, R. Zhao, Y.C. Yeo, T.C. Chong, and S.R. Elliott, *Science* **336**, 1566 (2012).
- ⁴ A. Chanthbouala, A. Crassous, V. Garcia, K. Bouzehouane, S. Fusil, X. Moya, J. Allibe, B. Dlubak, J. Grollier, S. Xavier, C. Deranlot, A. Moshar, R. Proksch, N.D. Mathur, M. Bibes, and A. Barthélémy, *Nat. Nanotech* **7**, 101 (2012).
- ⁵ E.Y. Vedmedenko, R.K. Kawakami, D.D. Sheka, P. Gambardella, A. Kirilyuk, A. Hirohata, C. Binek, O. Chubykalo-Fesenko, S. Sanvito, B.J. Kirby, J. Grollier, K. Everschor-Sitte, T. Kampfrath, C.-Y. You, and A. Berger, *J. Phys. D: Appl. Phys.* **53**, 453001 (2020).
- ⁶ L. Stojchevska, I. Vaskivskyi, T. Mertelj, P. Kusar, D. Svetin, S. Brazovskii, and D. Mihailovic, *Science* **344**, 177 (2014).
- ⁷ I. Vaskivskyi, I.A. Mihailovic, S. Brazovskii, J. Gospodaric, T. Mertelj, D. Svetin, P. Sutar, and D. Mihailovic, *Nat. Commun.* **7**, 11442 (2016).
- ⁸ D. Mihailovic, D. Svetin, I. Vaskivskyi, R. Venturini, B. Lipovšek, and A. Mraz, *Appl. Phys. Lett.* **119**, 013106 (2021).
- ⁹ A. Mohammadzadeh, S. Baraghani, S. Yin, F. Kargar, J.P. Bird, and A.A. Balandin, *Appl. Phys. Lett.* **118**, 093102 (2021).
- ¹⁰ A. Mraz, R. Venturini, M. Diego, A. Kranjec, D. Svetin, Y. Gerasimenko, V. Sever, I.A. Mihailovic, J. Ravnik, I. Vaskivskyi, M. D'Antuono, D. Stornaiulo, F. Tafuri, D. Kazazis, Y. Ekinci, and D. Mihailovic, *ArXiv:2103.04622* (2021).
- ¹¹ M. Yoshida, R. Suzuki, Y. Zhang, M. Nakano, and Y. Iwasa, *Sci. Adv.* **1**, e1500606 (2015).
- ¹² G. Gruner, *Rev. Mod. Phys.* **60**, 53 (1988).
- ¹³ K. Rossnagel, *J. Phys. Condens. Matter* **23**, 213001 (2011).
- ¹⁴ B. Sipos, A.F. Kusmartseva, A. Akrap, H. Berger, L. Forró, and E. Tutiš, *Nat. Mater.* **7**, 960 (2008).
- ¹⁵ A.F. Kusmartseva, B. Sipos, H. Berger, L. Forró, and E. Tutiš, *Phys. Rev. Lett.* **103**, 236401 (2009).
- ¹⁶ C. Berthier, P. Molinié, and D. Jérôme, *Solid State Commun.* **18**, 1393 (1976).
- ¹⁷ E. Morosan, H.W. Zandbergen, B.S. Dennis, J.W.G. Bos, Y. Onose, T. Klimczuk, A.P. Ramirez, N.P. Ong, and R.J. Cava, *Nat. Phys.* **2**, 544 (2006).
- ¹⁸ L.J. Li, W.J. Lu, X.D. Zhu, L.S. Ling, Z. Qu, and Y.P. Sun, *EPL* **97**, 67005 (2012).
- ¹⁹ Y. Liu, R. Ang, W.J. Lu, W.H. Song, L.J. Li, and Y.P. Sun, *Appl. Phys. Lett.* **102**, 192602 (2013).
- ²⁰ A. Kogar, A. Zong, P.E. Dolgirev, X. Shen, J. Straquadine, Y.-Q. Bie, X. Wang, T. Rohwer, I.-C. Tung, Y. Yang, R. Li, J. Yang, S. Weathersby, S. Park, M.E. Kozina, E.J. Sie, H. Wen, P. Jarillo-Herrero, I.R. Fisher, X. Wang, and N. Gedik, *Nat. Commun.* **16**, 159 (2020).
- ²¹ N. Yoshikawa, H. Suganuma, H. Matsuoka, Y. Tanaka, P. Hemme, M. Cazayous, Y. Gallais, M. Nakano, Y. Iwasa, and R. Shimano, *Nat. Phys.* **17**, 909 (2021).

- ²² X. Wang, Z. Song, W. Wen, H. Liu, J. Wu, C. Dang, M. Hossain, M.A. Iqbal, and L. Xie, *Adv. Mater.* **31**, 1804682 (2019).
- ²³ G. Liu, B. Debnath, T.R. Pope, T.T. Salguero, R.K. Lake, and A.A. Balandin, *Nature Nanotech* **11**, 845 (2016).
- ²⁴ L. Ma, C. Ye, Y. Yu, X.F. Lu, X. Niu, S. Kim, D. Feng, D. Tománek, Y.-W. Son, X.H. Chen, and Y. Zhang, *Nat. Commun.* **7**, 10956 (2016).
- ²⁵ Y.A. Gerasimenko, P. Karpov, I. Vaskivskiy, S. Brazovskii, and D. Mihailovic, *Npj Quantum Mater.* **4**, 1 (2019).
- ²⁶ I. Vaskivskiy, J. Gospodaric, S. Brazovskii, D. Svetin, P. Sutar, E. Goreshnik, I.A. Mihailovic, T. Mertelj, and D. Mihailovic, *Sci. Adv.* **1**, e1500168 (2015).
- ²⁷ J. Ravnik, I. Vaskivskiy, T. Mertelj, and D. Mihailovic, *Phys. Rev. B* **97**, 075304 (2018).
- ²⁸ D.H. Auston, *Appl. Phys. Lett.* **26**, 101 (1975).
- ²⁹ M.B. Ketchen, D. Grischkowsky, T.C. Chen, C. Chi, I.N. Duling, N.J. Halas, J. Halbout, J.A. Kash, and G.P. Li, *Appl. Phys. Lett.* **48**, 751 (1986).
- ³⁰ G.A. Mourou and K.E. Meyer, *Appl. Phys. Lett.* **45**, 492 (1984).
- ³¹ J. Serafini, A. Hossain, R.B. James, M. Guziewicz, R. Kruszka, W. Słysz, D. Kochanowska, J.Z. Domagala, A. Mycielski, and R. Sobolewski, *Appl. Phys. Lett.* **111**, 011108 (2017).
- ³² D.R. Dykaar, R. Sobolewski, and T.Y. Hsiang, *IEEE Trans. Magn.* **25**, 1392 (1989).
- ³³ F.A. Hegmann, D. Jacobs-Perkins, C. -C. Wang, S.H. Moffat, R.A. Hughes, J.S. Preston, M. Currie, P.M. Fauchet, T.Y. Hsiang, and R. Sobolewski, *Appl. Phys. Lett.* **67**, 285 (1995).
- ³⁴ R. Adam, M. Currie, C. Williams, R. Sobolewski, O. Harnack, and M. Darula, *Appl. Phys. Lett.* **76**, 469 (2000).
- ³⁵ C. Kastl, C. Karnetzky, H. Karl, and A.W. Holleitner, *Nat Commun* **6**, 6617 (2015).
- ³⁶ J.W. McIver, B. Schulte, F.-U. Stein, T. Matsuyama, G. Jotzu, G. Meier, and A. Cavalleri, *Nat. Phys.* **16**, 38 (2020).
- ³⁷ Y. Yang, R.B. Wilson, J. Gorchon, C.-H. Lambert, S. Salahuddin, and J. Bokor, *Sci. Adv.* **3**, e1603117 (2017).
- ³⁸ K. Jhuria, J. Hohlfeld, A. Pattabi, E. Martin, A.Y. Arriola Córdova, X. Shi, R. Lo Conte, S. Petit-Watelot, J.C. Rojas-Sanchez, G. Malinowski, S. Mangin, A. Lemaître, M. Hehn, J. Bokor, R.B. Wilson, and J. Gorchon, *Nat Electron* **3**, 680 (2020).
- ³⁹ J.K. Furdyna, *J. Appl. Phys.* **64**, R29 (1988).
- ⁴⁰ S.B. Trivedi, C.-C. Wang, S. Kutcher, U. Hommerich, and W. Palosz, *J. Cryst. Growth* **310**, 1099 (2008).
- ⁴¹ J. Vodeb, V.V. Kabanov, Y.A. Gerasimenko, R. Venturini, J. Ravnik, M.A. van Midden, E. Zupanec, P. Sutar, and D. Mihailovic, *New J. Phys.* **21**, 083001 (2019).
- ⁴² S. Perkowitz and R.H. Thorland, *Phys. Rev. B* **9**, 545 (1974).

⁴³ D.S. Holmes, A.L. Ripple, and M.A. Manheimer, IEEE Trans. Appl. Supercond. **23**, 1701610 (2013).

⁴⁴ O.A. Mukhanov, IEEE Transactions on Applied Superconductivity **21**, 760 (2011).

⁴⁵ Y. Chen, W. Ruan, M. Wu, S. Tang, H. Ryu, H.-Z. Tsai, R. Lee, S. Kahn, F. Liou, C. Jia, O.R. Albertini, H. Xiong, T. Jia, Z. Liu, J.A. Sobota, A.Y. Liu, J.E. Moore, Z.-X. Shen, S.G. Louie, S.-K. Mo, and M.F. Crommie, Nat. Phys. **16**, 218 (2020).

⁴⁶ X. Wang, H. Liu, J. Wu, J. Lin, W. He, H. Wang, X. Shi, K. Suenaga, and L. Xie, Adv. Mater. **30**, 1800074 (2018).